This is the Pre-Published Version.

Y.H. Liu, L. Zhang, Y.F. Ding, X.J. Huang, X.Y. Huang (2024) *Effect of Thermal Impact on the Onset and Propagation of Thermal Runaway over Cylindrical Li-ion Batteries*, **Renewable Energy**, 119910. https://doi.org/10.1016/j.renene.2023.119910

Effect of Thermal Impact on the Onset and Propagation of Thermal Runaway over Cylindrical Li-ion Batteries

Yanhui Liu[a,b], Lei Zhang[a], Yifei Ding[a], Xianjia Huang[c], Xinyan Huang[a,b,*]

[a] *Dept of Building Environment and Energy Engineering, The Hong Kong Polytechnic University, HK*

[b] *The Hong Kong Polytechnic University Shenzhen Research Institute, Shenzhen, China*

[c] *Guangzhou Institute of Industrial Technology, Guangzhou, China*

**Corresponding to xy.huang@polyu.edu.hk (X. Huang)*

Abstract: The external heating test is widely used to evaluate the hazards of battery thermal runaway, but the efficiency and effect of the heating source are rarely quantified. This work performs thermal runaway propagation tests in a 3-layer cylindrical battery pile with a uniform state of charge (SOC) ranging from 30% to 75%. A cylindrical heater is in contact with two cells in the first layer and has a power varying from 50 W to 300 W to trigger thermal runaway. Results indicate that for the current system, the heating efficiency to a single cell is around 15%, and the effective heating power is insensitive to the SOC. The intensity of thermal runaway increases with the external heating power and the cell SOC. The influence of external heating on the propagation of thermal runaway is reflected in the intensity of thermal runaway in the first-layer cells and the preheating effect of subsequent layers. A simplified heat-transfer model is established to quantify the thermal impact on both thermal runaway intensity and preheating depth. Finally, a new approach for selecting the appropriate heating power is proposed to help optimize battery thermal-runaway tests and improve the safety regulations for modules.

Keywords: *Energy storage; Battery safety; Heating abuse; Heating power; Fire spread*

Nomenclature

Symbols		***Subscripts***	
A	area [m^2]	*a*	ambient
c	specific heat [J/(kg·K)]	*c*	cooling
h	heat transfer coefficient [W/(m^2·K)]	*d*	depth direction
k	thermal conductivity [W/(m·K)]	*ex*	external
m	mass [g]	*in*	inside
$\dot{q}$	heating/cooling rate [W]	*L*	layer
t	time [s]	*LIB*	lithium-ion battery
T	temperature [°C]	*max*	maximum
Greeks		**Abbreviations**	
α	thermal diffusion coefficient	*LIB*	lithium-ion battery
δ	thermal penetration depth [m]	*SOC*	state of charge
ρ	density [kg/m^3]	*TR*	thermal runaway

1. Introduction

Lithium-ion battery (Li-ion battery or LIB) is a promising energy-storage solution in combating climate change and achieving carbon neutrality. The market demand for LIBs has been increasing rapidly, with widespread applications ranging from portable electronic devices to electric vehicles and grid-scale energy storage systems. However, safety issues related to battery thermal runaway still act as significant obstacles hindering the further development and application of LIBs [1]. The frequent battery and electric vehicle (EV) fires require more research on the thermal runaway characteristics of LIBs and better fire safety measures for the battery energy storage system [2,3].

Thermal runaway is one of the most catastrophic failure modes of LIB, usually accompanied by violent combustion or even an explosion [4–6]. It occurs when the rate of internal heating caused by chemical reactions within the battery greatly exceeds the cooling rate of the surrounding environment [7]. Given that the LIB components have relatively low thermal stability, thermal runaway can be triggered by several abuse conditions, mainly including thermal abuse [8], mechanical abuse [9], and electrical abuse [10]. During the overheating abuse, the thermal decomposition of the solid electrolyte interface (SEI) layer can be initiated over 69 °C [11]. Afterwards, the reaction between anode and electrolyte would happen, increasing the cell temperature and further inducing other exothermic reactions. If the environmental cooling rate is low, the heat will accumulate inside the cell and continue to increase the cell temperature. Once the cell temperature reaches a certain threshold, a significant amount of heat and smoke will be released sharply, resulting in thermal runaway [12–14]. In practice, thousands of cells are closely arranged in the battery pack to meet the capacity requirements. Consequently, thermal runaway propagation throughout the entire pack presents the most severe scenario for battery fires [15,16].

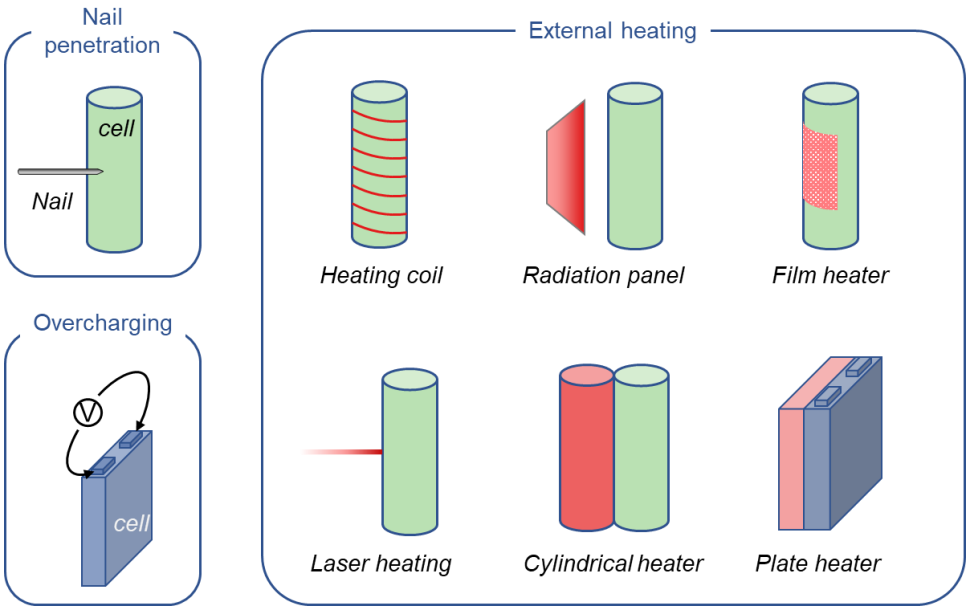

Fig. 1. The commonly used methods to trigger the battery thermal runaway.

The most common approach to thermal runaway propagation testing is to induce thermal runaway in a single cell or layer-to-layer over multiple cells and study how it propagates through the battery modules [17–19]. The results can evaluate the safety resilience of the LIB module and guide the fire-safety design. In the literature, the initiation methods for thermal runaway comprise external heating, overcharging, and nail penetration (Fig. 1). Among them, external heating is perceived as the optimal triggering method with excellent repeatability [20,21]. According to the different heat transfer modes, external heating can be divided into radiative heating using a laser or radiation panel and conductive heating via contacted heaters. In literature, conductive heating is commonly used due to simple design.

The heater utilized to trigger battery thermal runaway depends on the cell shape. Specifically, the film heater [22–24], cylindrical heater [25–31], and heating coil [32,33] are typically used for the cylindrical cells, whereas the plate heater [34–36] is usually employed for prismatic and pouch cells. Moreover, selected thermal impact (usually represented by the power of a specific heater) in literature was primarily chosen according to some specification standards and regulations. For example, the criteria for heater power selection in some standards are listed in Table 1 [37,38].

For cylindrical or plate heaters, the standards only provide maximum heater power associated only with the cell energy, and their values vary in a large range. This is very different from mature ignition and fire tests, which define a minimum or fixed heat flux received by the fuel rather than giving a vague value of some heater power [39]. The lack of more specific test standards is because the scientific community still does not know enough about the effect and efficiency of external heating on the battery and the consequent onset and propagation of thermal runaway.

Table 1. The heater power selection recommended by some standards.

Standard code	Heating method	Basis for heating power selection
IEC 62619-2022	Heater/burner/inductive heating	Not mentioned
UL 9540A-2019	Flexible film heaters	Cell surface heating rate should be 4 to 7 °C/min
GB 38031-2020	Cylindrical or plate heater	Depends on cell energy capacity. For example, the maximum heater power for a cell with an energy capacity lower than 100 Wh should range from 30 to 300 W (Table. A1).

In the literature, the heater powers used to trigger cell-to-cell [29,30] or layer-to-layer [26–28] thermal runaway propagation are also various. Although past research has studied the heating-power impact on the thermal runaway of a single cell [40,41], its influence on thermal runaway propagation in battery modules is still unclear. Zhong *et al*. [26] utilized a cylindrical heater of 100~400 W to study the thermal runaway propagation within a linear battery module. Despite the varying levels of heating power used, the cell-to-cell thermal runaway propagation did not occur in the linear battery module consisting of 3 cells. However, layer-to-layer thermal runaway propagation was observed in the 9-cell

battery modules. Recently, Jin *et al*. [42] explored the impact of heating power on thermal runaway propagation in prismatic battery modules. The study employed seven different heating powers and revealed the preheating effect as the primary cause of acceleration in thermal runaway propagation. However, previous studies mainly tested fully charged cells under relatively high heating powers. The understanding of the preheating effect in battery modules with a low state of charge (SOC) is still limited. Meanwhile, the literature still lacks exploring such a thermal impact on the measured limiting condition and the rate of thermal runaway propagation, so there is a knowledge gap.

This work investigated the thermal runaway propagation for 18650-type cells with various SOCs. Thermal runaway propagation was initiated by a cylindrical heater with a power of 50~300 W. Effects of heating power and SOC level on thermal runaway propagation were comprehensively investigated. The critical conditions for thermal runaway propagation in cells with low SOC were demonstrated and theoretically elucidated for the first time. Finally, the selection strategy of heater power was proposed by considering the heating energy input and potential thermal runaway propagation rate. These findings can provide scientific guidelines for optimizing future battery test procedures in the safety regulations.

2. Experimental setup

2.1. Battery samples

The commercial 18650-type LIB (ICR18650-22F, Samsung SDI Co., Ltd) with a 2.2-Ah nominal capacity was selected in this work. It has the cathode material of $LiNi_{0.5}Co_{0.2}Mn_{0.3}O_2$ (NCM 523) and the anode material of intercalation graphite. Prior to the tests, the SOC level for each cell was calibrated using a battery test system (5 V/12 A, ± 6 mA, Neware). The LIB information and SOC calibration parameters are summarized in Table 2. Specifically, cells were first charged using a constant current (CC) of 1100 mA to a maximum cut-off voltage of 4.2 V and then charged at constant voltage (CV) mode until the current decreased to lower than 110 mA. Finally, cells were discharged to the prescribed SOC levels at a constant current of 1100 mA. To avoid the effects of internal heating caused by battery cycling, cells were rested for at least two hours at room temperature after the SOC calibration process.

Table 2. Specifications of the LIB samples in this work.

Parameters	**Battery cell**
Cathode	$Li(Ni_{0.5}Co_{0.2}Mn_{0.3})O_2$
Anode	Graphite
Nominal capacity (Ah)	2.2
Nominal voltage (V)	3.6
Mass (g)	41.0 ± 0.5
Minimum cut-off Voltage (V)	2.75 ± 0.05
Maximum cut-off Voltage (V)	4.20 ± 0.05
Constant current for charging/discharging (mA)	1100
Cut-off current for charging (mA)	110
Prescribed SOC level	30%, 50%, and 75%

Previous studies found that thermal runaway consistently exhibits ordered propagation patterns in the first few cells of the actual battery systems [43]. Thus, small-scale modules with several cells or layers were primarily employed in literature to investigate the characteristics of thermal runaway propagation. Inspired by recent studies on battery thermal safety [44–46], the typical 2×3 module design of 18650-type cells was employed in this work. Additionally, thermal runaway propagation in a real battery system could take on a three-dimensional path. However, since our primary focus in this study was on the effects of heating power and state of charge (SOC) level, we simplified the battery module and only considered horizontal propagation.

2.2. Experimental apparatus

Fig. 2 illustrates the experimental setup of this work. The tests were carried out in a quiescent chamber to minimize the influence of environmental wind. A cylindrical heater with an equivalent dimension to the LIB cell was utilized to initiate the thermal runaway of adjacent cells. This heating method has been employed in many previous studies and standards [28]. The heating power was adjusted by a DC power supply (MS-DMP-D) and ranged from 50 W to 300 W [37,38]. The stainless-steel wires were employed to anchor the LIB stockpile to secure tight contact between the heater and cells. During the tests, the fixed LIB cells and the heater were placed on an electronic balance (GX-10K, A&D Company). The balance can output mass data to the integrated computer with a frequency of 10 Hz. Except for the mass information, the temperatures of the heater (T_h), LIB cell (T_{LIB}), and ambient (T_a) were measured using tiny K-type thermocouples with the 2-mm beads and ± 0.1 °C accuracy. The temperature evolution was recorded by a data logger (HIOKI LR8400) with a data-acquisition rate of 1 Hz. The entire process of thermal runaway propagation was captured by a video camera (SONY FDR-AX40, 25 fps) and an infrared camera (FLIR E85).

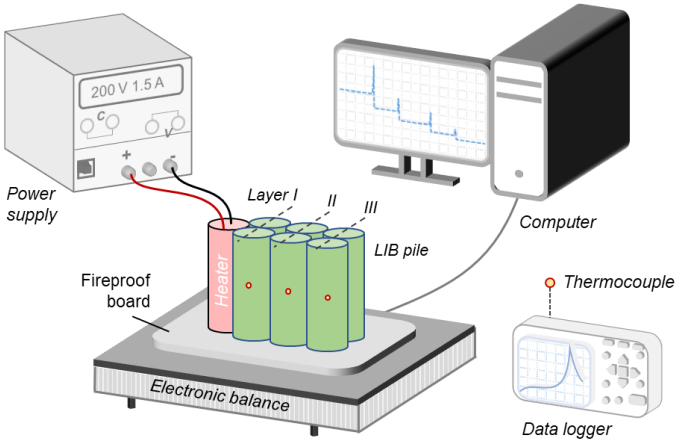

Fig. 2. The schematic diagrams of the experimental setup.

2.3. Testing procedures and controlling parameters

Prior to the experiment, fireproof boards were affixed to the electronic balance to prevent potential damage from battery thermal runaway. Subsequently, the electronic scale was zeroed, and the battery stack was cautiously positioned on the fireproof boards. Afterwards, the DC power supply and data

acquisition systems were simultaneously activated to start the tests. After the heating, the experimental phenomena and cell temperatures were continuously observed. The heater was promptly turned off when rapid temperature rise was found in the first-layer LIBs caused by thermal runaway.

The experiments were terminated once the temperature of all cells had sufficiently decreased to a safe value of about 50 °C for handling. To reduce experimental uncertainty, each case was repeated at least twice. In this work, two key controlled parameters for the layer-to-layer thermal runaway propagation tests are listed as follows.

(I) Triggering heating power. Five powers of 50 W, 100 W, 150 W, 200 W, and 300 W were selected for the heater. The DC power supply was used to maintain a constant heating power, where the current and voltage parameters were pre-calibrated accordingly.

(II) Cell SOC level. LIB cells with SOC levels of 30%, 50%, and 75% were adopted for thermal runaway propagation tests. It should be noted that 30% is the highest recommended SOC value for LIBs during storage and transport [47]. Moreover, previous studies indicated that LIBs with a SOC level of approximately 70% could exhibit the most significant thermal runaway propagation ability [48]. Thus, cells with 30%, 50%, and 75% SOC were selected.

3. Results

3.1. Experimental phenomena

The typical experimental phenomena of the heating tests are demonstrated in Fig. 3. Upon turning on the heater, its temperature rapidly increases, thereby heating the Layer-I cells. Once the thermal runaway of Layer-I cells is induced, the heater will be turned off. Then, the layer-to-layer propagation of thermal runaway can be observed in the video snapshots and thermal images.

Fig. 3a presents the thermal behaviors of 75% SOC cells with a heater power of 300 W. The heater heats the Layer-I cells in the first 2 minutes and 30 seconds (2’30”). During this period, the exothermic reactions inside the cells are activated as their temperature rises. When the thermal runaway of Layer-I cells is triggered, large amounts of smoke and sparks are ejected from the positive pole. The sparks quickly ignite the flammable gases, forming a bright flame (Video S1). Under the heating of failed Layer-I cells, the flaming combustion caused by the thermal runaway of Layer-II cells is observed at around 5’23”. Finally, thermal runaway successfully propagates through the entire LIB pile, and all LIB cells are burnt out.

Thermal runaway propagation of 50% SOC cells with 300-W heater power is shown in Fig. 3b. The external heating time for Layer-I cells is about 3’15”, a little bit longer than that of 75% SOC cells. Afterward, the thermal runaway of LIB cells successively occurs, where no jetting flame is observed (Video S2). This is because the thermal runaway of low-SOC cells releases relatively less heat and flammable gas, which is not enough to form flaming combustion. The thermal images of 50% SOC cells also suggest that the maximum temperature is much lower, agreeing with previous studies [49].

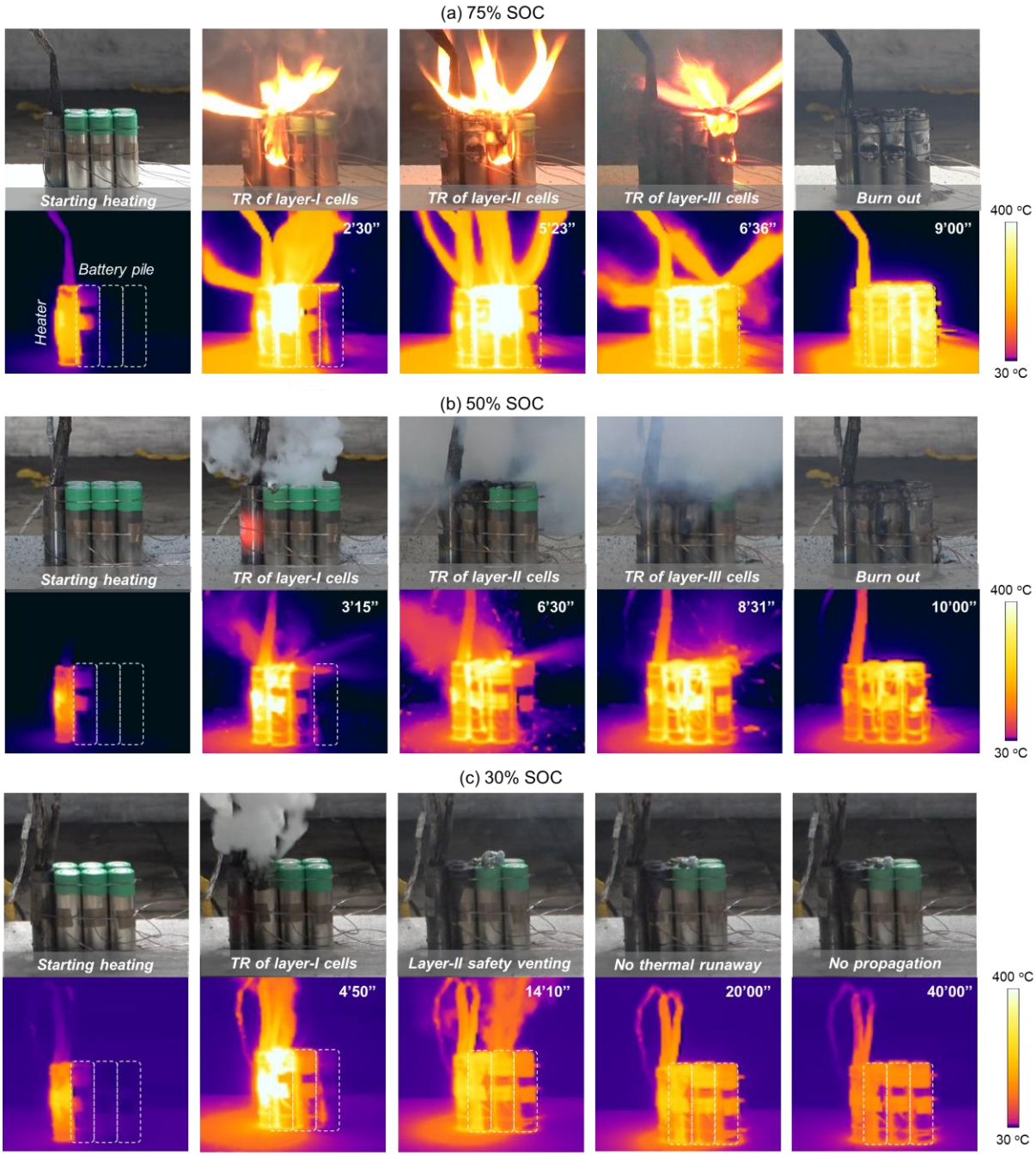

Fig. 3. Snapshots from the video footage of the (a) 75% SOC cells with a 300-W heater, (b) 50% SOC cells with a 300-W heater, and (c) 30% SOC cells with a 200-W heater.

Regarding 30%-SOC cells, the thermal runaway cannot propagate if it is triggered by a heater power of 200 W (Fig. 3c). Thermal runaway of Layer-I cells happens at about 4'50'', accompanied by considerable white smoke and no visible flame (Video S3). According to the video snapshots and thermal images, the intensity of thermal runaway for 30%-SOC cells is much weaker. At 14'10'', the safety valve of Layer-II cells opens, indicating that some decomposition reactions inside the Layer-II cells have been initiated. However, the heat accumulation inside the cells is not enough to further trigger the thermal runaway. Finally, the cells in Layer-II and Layer-III are cooled down by the environment.

3.2. Temperature and mass evolution

To further analyze the thermal runaway propagation behaviors, Fig. 4 shows the evolution curves of mass and temperature for the LIB piles with a 300-W heater. The initial temperature of cells is around 28 °C, and the initial weight of the LIB pile is 340 g. For 75% SOC cells in Fig. 4a, the temperature of Layer-I cells gradually rises with an average rate of 0.9 °C/s after the heater starts. A noticeable temperature gradient can be found in the LIB pile, where the temperature of Layer-II and Layer-III cells remains the initial value.

After heating for about 2 min, a rapid temperature increase can be found for LIB-1 and LIB-2. This is attributed to the micro short circuit inside the cell when the separator starts to melt. Afterward, the large-scale internal short circuit and heat release would be caused [40]. As the cell temperature continues to rise, the thermal runaway of LIB-2 and LIB-1 successively occurs within a short time interval. During the thermal runaway, large amounts of gases and sparks are released from the cells, and the reacting force of the violent gas jet causes the value of electronic balance to rise rapidly. After turning off the heater, thermal runaway propagates through the Layer-II and Layer-III cells in 4 min. Finally, the total mass loss for this case is approximately 64 g, and the maximum temperature for 75% SOC cells during the thermal runaway is higher than 800 °C.

In this work, the temperature rising rate of over 5 °C/s lasting longer than 5 s has been established as the benchmark for identifying the onset of thermal runaway. Such a criterion considered the battery temperature gradient along the layers, which is further confirmed by experimental observations [22]. The average thermal runaway time of the cells within the layer is calculated as the layer-based thermal runaway time. Therefore, the layer-to-layer propagation time can be identified approximately. As shown in Fig. 4a, the thermal runaway propagation time from Layer-I to Layer-II ($\overline{\Delta t_1}$) is 156 s, while the propagation time from Layer-II to Layer-III ($\overline{\Delta t_2}$) is 82 s. This acceleration phenomenon of thermal runaway propagation can be found in LIB modules with high SOC level, which has been reported by many previous studies [38].

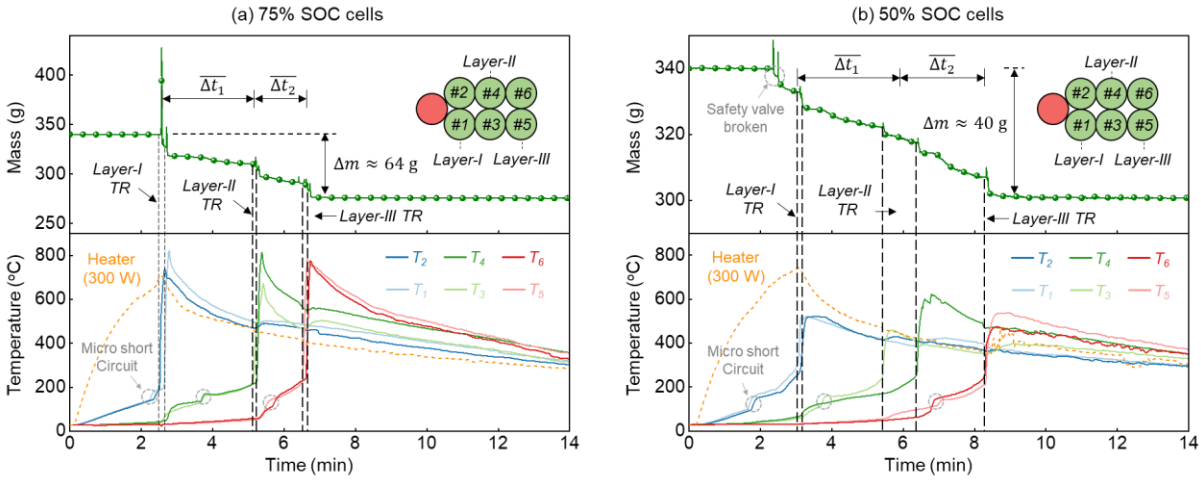

Fig. 4. Temperature and mass evolution of cells with (a) 75% SOC and (b) 50% SOC under the 300-W heater.

In terms of the 50% SOC LIB pile with a 300-W heater, the temperature and mass variation curves are depicted in Fig. 4b. For Layer-I cells, the temperature rise caused by the micro short circuit is also observed at around 2 min. Then, the cell temperature increases relatively slowly, indicating a lower heat generation rate within the 50% SOC cells. At about 2'30", there is a slight decrease in the battery temperature caused by heat loss through the opening of the safety valve. The safety valve break also results in a transient increase in the mass curve due to the counteracting force generated. Despite the safety valve opening, heat continues to accumulate inside the battery. The Layer-I cells experience thermal runaway at approximately 3 min, with a maximum surface temperature of 525 °C. Overall, it takes 170 s for the thermal runaway to propagate from Layer-I to Layer-II and 140 s from Layer-II to layer-III. The longer thermal runaway propagation time and less mass loss observed in Fig. 4b suggest that the thermal hazards of 50% SOC cells are much smaller.

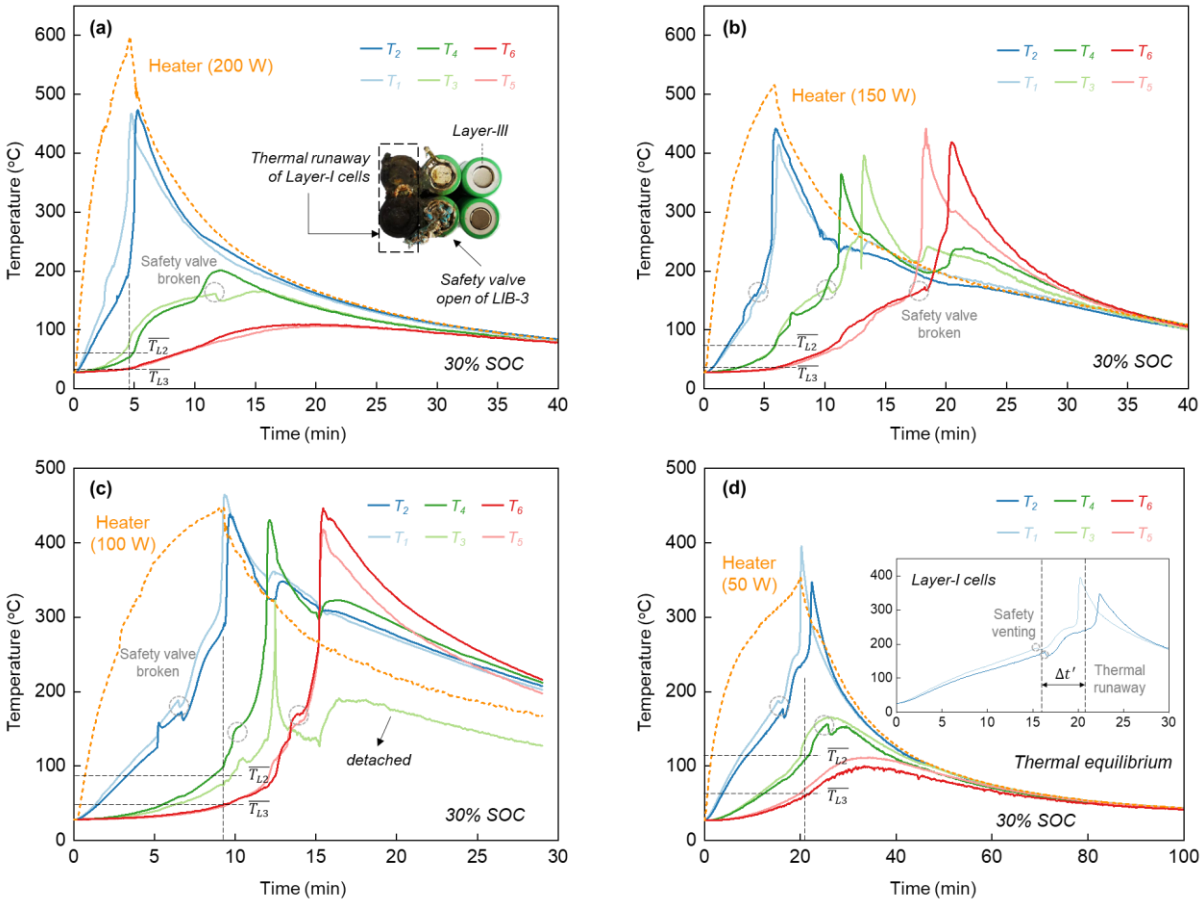

Fig. 5. Temperature variations of 30% SOC cells with the heater power of (a) 200 W, (b) 150 W, (c) 100 W, and (d) 50 W.

For cells with 30% SOC, Fig. 5 shows the temperature responses under various heating conditions. The temperature variations displayed in Fig. 5a correspond to the experimental condition of Fig. 3c, where the heater power was set at 200 W. A significant temperature gradient is observed within the LIB pile after the initiation of heating. After around 5-min heating, the Layer-I cells undergo thermal

runaway. The maximum temperature for the cell surface during the thermal runaway is approximately 470 °C, which is significantly lower than that of the cells at both 50% and 75% SOC. When the thermal runaway occurs in Layer-I cells, the average temperature of Layer-II cells ($\overline{T_{L2}}$) is 67 °C, and the average temperature of Layer-III cells ($\overline{T_{L3}}$) is 39 °C. After the thermal runaway in Layer-I cells, the temperature of the Layer-II cells gradually increased. The safety valve of the LIB-3 is broken at around 11 min. Despite being heated to 200 °C, no thermal runaway happens in the Layer-II cells. Eventually, all cells slowly returned to ambient temperature due to the cooling effect of the environment.

Employing a lower heating power, Fig. 5b indicates that thermal runaway successfully propagates through the LIB pile with a 150-W heater. In addition, the opening of the safety valve can also be observed in the temperature curves of Layer-I cells. Before turning off the heater, the average temperature of Layer-II cells ($\overline{T_{L2}}$) is 78 °C, about 11 °C higher than the value of $\overline{T_{L2}}$ in Fig. 5a. This is caused by the "preheating" effect. Specifically, the heater with lower power takes a long time to heat Layer-I cells to their thermal-runaway threshold so that the heat can penetrate Layer-I cells and increase the average temperature of Layer-II cells. Thus, the propensity of thermal runaway propagation is significantly increased, which could be caused by such a "preheating" effect. Similarly, thermal runaway propagation occurs in the 30%-SOC LIBs with a 100-W heater, as shown in Fig. 5c and Video. S4. A relatively high value of $\overline{T_{L2}}$ and shorter thermal runaway propagation time can be observed, which is also the result of "preheating" and will be discussed further.

When the heater power is 50 W, the value of $\overline{T_{L2}}$ is around 78 °C (Fig. 5d), much higher than that of cases with high heating power. Nevertheless, thermal runaway cannot propagate in the entire LIB pile, which is ascribed to the net thermal energy obtained by Layer-II cells being insufficient to initiate thermal runaway. Specifically, low heating power prolongs the time interval between safety venting and thermal runaway of Layer-I cells, leading to the relatively weak thermal runaway intensity of LIB cells [50]. Meanwhile, the turned-off heater would also absorb heat from Layer-I cells after thermal runaway [42], as the maximum temperature of the low-power heater is lower than that of the Layer-I cells after the thermal runaway. Consequently, the heat transfer to Layer-II cells is low in Fig. 5d, so no thermal runaway propagation occurs.

Fig. 6 summarizes the mass loss of the thermal-runaway cells under different heating conditions. The mass loss ratio is also calculated to analyze the effects of heater power and SOC. It is apparent that the mass loss increases with the SOC level, which is consistent with previous studies [40]. Specifically, when the heater power is 300 W, the mass loss ratio of a single cell increases from 14.4% (~5.9 g) to 26.3% (~10.8 g) as the SOC increases from 30% to 75%. This is because higher SOC cells can reach more severe thermal runaway, agreeing with the observation of more ejected materials during the tests. Moreover, Fig. 6 also suggests that the mass loss fraction for 30% SOC cells slightly increases with heater power. As the heater power increases from 50 W to 300 W, the mass loss ratio of a single cell increases from 10.0% (~4.1 g) to 14.4% (~5.9 g). For cells with 50% and 75% SOC, the mass loss is

insensitive to the heater power, even though the time interval between safety venting and thermal runaway shows an enlarging trend with the heater power. The following sections will provide a detailed discussion to explain the aforementioned trends.

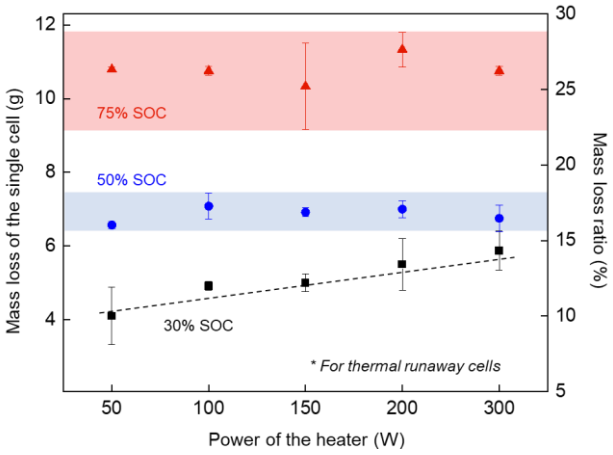

Fig. 6. Average mass loss and the corresponding mass-loss ratio of a thermal-runaway cell vs. heating power.

3.3. Features of thermal runaway initiation

Determining the actual heating rate is essential to reveal the thermal impact of a heater on the onset of thermal runaway. For the battery module with a 300-W heater, Fig. 7a shows the temperature rising rate of the first thermal-runaway cell with various SOCs. The temperature rising rate first increases and then remains at a specific value. Afterwards, two peaks can be observed for each evolution curve, caused by micro short circuit and thermal runaway, respectively. The maximum temperature rising rate during thermal runaway significantly increases with the SOC, indicating a strong thermal runaway intensity. Before the first peak induced by the micro short circuit or the melting of the separator, the influence of reactions within the cell on its temperature is negligible. Thus, the average rate of temperature rise caused by the heater is insensitive to SOC level and is approximately 0.92 °C/s in Fig. 7a.

Fig. 7b further illustrates the thermal impact on the temperature rate of 30% SOC cells. The onset time of thermal runaway delays as the heater power decreases. Similarly, the temperature rising rate first increases and then remains at a certain value before the melting of the separator. As expected, such a certain value increases with the heater power. In Fig. 7b, the average temperature rise rate increases from 0.18 °C/s to 0.92 °C/s as heater power increases from 50 W to 300 W. Therefore, the effective heating rate ($\dot{q}_e$) can be estimated as

$$\dot{q}_e = c_{LIB} m \frac{dT}{dt} \tag{1}$$

where $c_{LIB} = 1100\ \mathrm{J/(kg \cdot K)}$ is cell specific heat, and m is the cell mass. Based on the experimental data, the estimated value for effective heating rate ($\dot{q}_e$) are listed in Table 3.

As the heater power increases from 50 W to 300 W, the effective heating power ($\dot{q}_e$) increases from 8.6 W to 42.2 W, with an increment of 390%. Regardless of the heater power, the heating efficiency is fixed to around 15.1% for one cell or 30.2% for two cells in Layer-I (Fig. 8). The heating efficiency is

mainly controlled by the shapes of the heater and cell, and the distance and contact between them, which do not change much with the power of the heater.

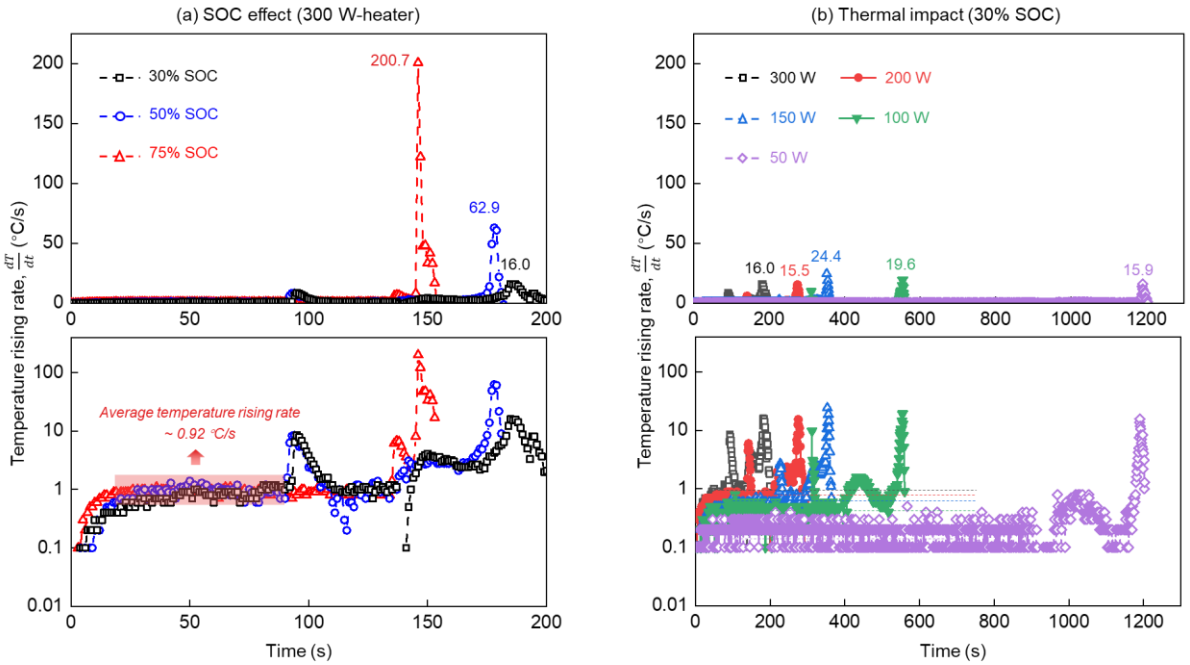

Fig. 7. Temperature rising rate of the first cell that reached the thermal runaway in the (a) battery module with various SOC levels and 300 W heaters and (b) 30% SOC battery module under various heating conditions.

Table 3. Calculation of the effective heating rate to the single cell.

Heater power (W)	Temperature rising rate (°C/s)	Effective heating power (W)	Efficiency of heating one cell (%)
50	0.19 ± 0.01	8.6 ± 0.8	17.2 ± 1.6
100	0.38 ± 0.02	17.1 ± 1.0	17.1 ± 1.0
150	0.48 ± 0.04	21.6 ± 2.0	14.4 ± 1.3
200	0.67 ± 0.02	30.3 ± 1.0	15.1 ± 0.5
300	0.94 ± 0.02	42.2 ± 0.9	14.1 ± 0.3

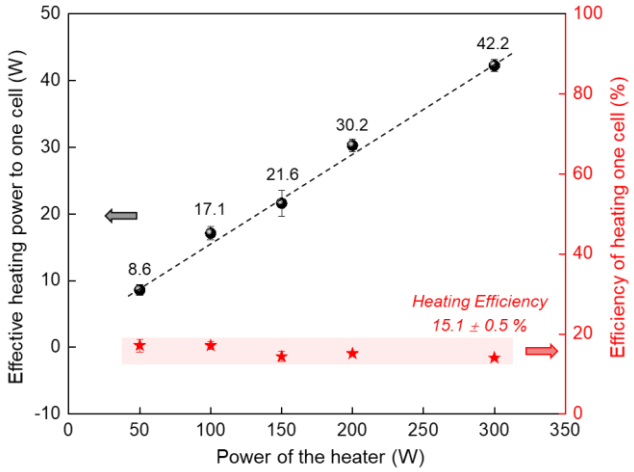

Fig. 8. The effective heating power of the cylindrical heater and the efficiency of heating one cell.

Fig. 9a shows the thermal runaway delay time of the Layer-I cells (t_1) varying with the heater power, whereas Fig. 9b describes the t_1 changing with calculated heating power. In this work, all heating powers could initiate the thermal runaway of Layer-I cells. The thermal runaway delay time (t_1) also represents the operating time of the heater. In Fig. 9a, heater power reduces its operation time, as the thermal runaway is always quickly triggered with a high-power heater [51].

In Fig. 9b, the value of t_1 displays a downward trend as SOC or heating power increases. For example, the thermal runaway delay time of 75% SOC cells decreases from 1,055 s to 150 s, as the effective heating power increases from 8.6 W to 42.2 W. When the effective heating power is 42.2 W (with the heater power of 300 W), the thermal runaway time reduces from 195 s to 150 s as the SOC increases from 30% to 75%. Moreover, the heating-power effect on thermal runaway time is more pronounced than SOC, agreeing with the findings reported by Zhang et al. [52]. Therefore, high heating power and high SOC levels can lead to a quick thermal runaway of Layer-I cells, and the heating-power effect is more dominant.

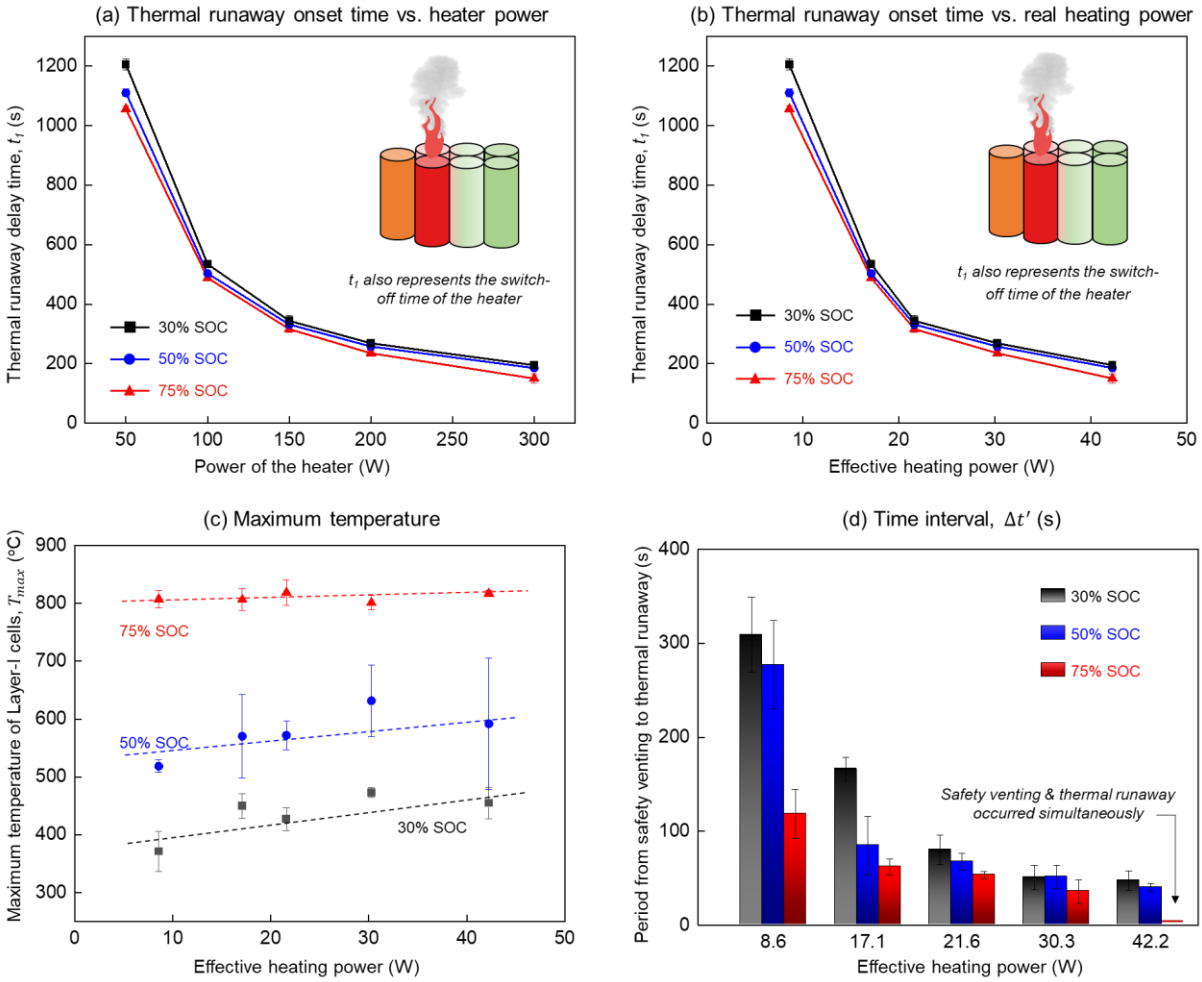

Fig. 9. Average thermal runaway (delay) time varying with (a) heater power and (b) effective heating power; (c) maximum temperature for Layer-I cells and (d) time interval between safety venting and thermal runaway under various heating power.

After the thermal runaway, the maximum surface temperatures of Layer-I cells are summarized in Fig. 9c. As expected, it increases with the SOC level [53]. The maximum temperature of cells with 30% and 50% SOC is much lower than that of 75% SOC cells, indicating a lower fire hazard. Additionally, the maximum temperature also increases with heating power, which is more evident for the low-SOC cells. For cells with 30% SOC, the maximum temperature rises by 22.4%, from 371 °C to 454 °C, as heating power increases from 8.6 W to 42.2 W. The slight upward trend of maximum temperature varying with heater power is consistent with the heating tests of prismatic cells delivered by Jin et al. [42]. The lower maximum temperature under low heating power could be attributed to the longer time interval between safety venting and thermal runaway. As shown in Fig. 9d, the time interval significantly decreases with the heating power. For 75% SOC cells, the safety venting and thermal runaway occur simultaneously under 42.2 W heating, while the time interval enlarges to 118 s under 8.6 W heating. Such a time interval can be regarded as the incubation of thermal runaway, which affects the heat accumulation inside the cells. Specifically, the more prolonged the time interval, the lower heat will be accumulated, resulting in a lower thermal runaway intensity [54]. Therefore, a higher heating power can lead to a more intensive thermal runaway, resulting in a higher maximum temperature, especially for low-SOC cells.

3.4. Characteristics of thermal runaway propagation

After the occurrence of the thermal runaway, the heater will be deactivated. Then, the capacity for thermal runaway propagation will be assessed. To quantify this capability in the LIB pile, a thermal runaway propagation rate is defined, indicating the number of layers that undergo thermal runaway per minute [layer/min] as

$$r = \frac{n}{\Delta t} \tag{2}$$

where Δt [min] stands for the time of thermal runaway propagation, and n [layer] represents the number of layers that reach thermal runaway. In literature, the value of r can help to understand the fire risk of the LIB module and provide strategies to mitigate the thermal hazards. Based on the experimental results, the mean propagation rate of thermal runaway varying with heating power is depicted in Fig. 10.

For cells with 75% SOC, the thermal runaway propagation rate slightly decreases with the heating power. As the heating power increases from 8.6 W to 42.2 W, the propagation rate is slowed by 43.8%. Such a trend is attributed to the “preheating” effect of Layer-I cells on subsequent cells [42]. In terms of 50% SOC cells, the rate of thermal runaway propagation decreases from 0.51 [layer/min] to 0. 39 [layer/min] as heater power increases from 8.6 W to 21.6 W. Further increasing the heating power, thermal runaway propagation becomes constant. This trend verifies the assumption that when the heating power is higher than a specific value, the “preheating” effect will be negligible. In this condition, the high heater power has little impact on thermal runaway propagation.

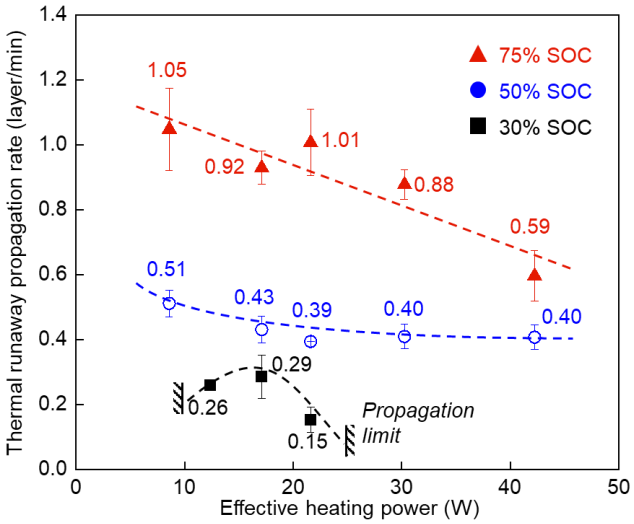

Fig. 10. Thermal runaway propagation rate varying with the heating power.

For cells with 30% SOC, thermal runaway propagation only occurred under the heating power ranging from 12.4 W to 21.6 W. Initially, thermal runaway can only propagate in the LIB pile with the heating power of 17.1 W and 21.6 W. The new test with a 75-W heater was further conducted to determine the lower propagation limit, and the real heating power is 12.4 W. The lower propagation limit could be ascribed to the less heat transferred from the Layer-I cells to Layer-II cells. On the one hand, low heating power will lead to a long incubation period, which attenuates the intensity of thermal runaway (Fig. 9d). On the other hand, when the thermal runaway of Layer-I cells happens, the temperature of the low-power heater is lower than the Layer-I cells. After the thermal runaway, the heater will absorb the heat from Layer-I cells, reducing the net heat transfer to Layer-II cells.

Moreover, a higher propagation limit for 30% SOC cells exists, corresponding to the heater power ranging from 21.6 W to 30.3 W (Fig. 10). It is attributed to the insufficient "preheating" of Layer-II cells. In other words, the temperature of Layer-II cells is still low when turning off the heater. The heat release from the thermal runaway of Layer-I cells is not enough to heat Layer-II cells to their thermal runaway threshold.

4. Discussions

4.1. Heat transfer analysis

To explicitly reveal the mechanisms of the thermal impact, this section will propose theoretical models explaining the trend of thermal runaway initiation and its propagation qualitatively. Fig. 11a provides a simplified heat transfer analysis for the thermal runaway initiation. The LIB pile is assumed to be a lumped system under an effective heating flux of $\dot{q}_e''$. Due to the configuration of the battery pile, a symmetric boundary is employed. At the critical condition for thermal runaway onset, the temperature of Layer-I cells reaches the threshold of thermal runaway (T_{TR}).

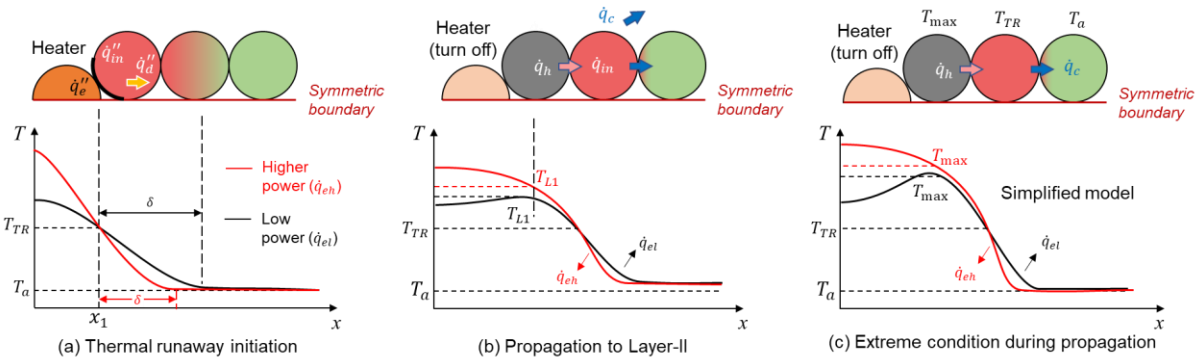

Fig. 11. Schematic diagram of simplified heat transfer model for (a) thermal runaway initiation of Layer-I cells, (b) thermal runaway propagation to Layer-II cells, and (c) extreme condition of low-SOC cells.

For the interface between the heater and LIB, the heat loss can be regarded as thermal conduction to subsequent cells ($\dot{q}_d''$). The heating sources mainly include external heating ($\dot{q}_e''$) and internal exothermic reactions ($\dot{q}_{in}''$). Then, the energy conservation equation can be expressed as

$$\dot{q}_e'' + \dot{q}_{in}'' = \dot{q}_d'' = -\left(k\frac{\partial T}{\partial x}\right)_{x=x_1} \tag{3}$$

where k is the effective thermal conductivity of the LIB pile in x direction. Under the side-heating, a thermal penetration depth (δ) can be defined to describe the "preheating" effect given by [55]

$$\delta = \sqrt{\alpha t_1} = \sqrt{\frac{kt_1}{\rho c_{LIB}}} \tag{4}$$

where α is the thermal diffusion coefficient; t_1 is the heating time, that is, the thermal runaway delay time of Layer-I cells; ρ is the density of LIB pile; and c_{LIB} is specific heat. Therefore, the triggering time for thermal runaway can be estimated as

$$t_1 \approx k\rho c_{LIB}\left(\frac{T_{TR}-T_a}{\dot{q}_e'' + \dot{q}_{in}''}\right)^2 \propto \left(\frac{1}{\dot{q}_e'' + \dot{q}_{in}''}\right)^2 \tag{5}$$

It should be noted that $\dot{q}_e''$ is the effective heating flux provided by the heater. $\dot{q}_{in}''$ can be determined through the Arrhenius equation, which is positively correlated with the SOC level. Thus, a higher heating power and SOC level can lead to a shorter thermal runaway time (Fig. 9a).

According to the temperature evolution curves, the temperatures of the heater and Layer-I cells start to drop after the thermal runaway, while the Layer-II cells continue to increase. As illustrated in Fig. 11b, when the thermal runaway of Layer-II cells occurs, the temperature of Layer-I cells (T_{L1}) is lower than its maximum temperature (T_{max}). Still, it will be higher than the heater temperature (T_h) if the initial heating power is low. The necessary condition for thermal runaway propagation from Layer-I to Layer II is that the temperature of Layer-II cells can be heated to T_{TR}. In other words, the total heating rate for Layer-II cells should be higher than the cooling rate ($\dot{q}_c$) at T_{TR} as

$$h_{TR}A(T_{L1} - T_{TR}) + \dot{q}_{in} \geq \dot{q}_c \tag{6}$$

where h_{TR} is the heat transfer coefficient from Layer-I and Layer-II; and A is effective heating area.

To analyze the "preheating" effect in low-SOC cells (50% and 30%), $\dot{q}_{in}$ could be negligible due to weak exothermic reactions. The extreme condition in Fig. 11c is considered to highlight the "preheating" impact and simplify the problems. In the simplified model, the temperatures of Layer-I, Layer II, and Layer-III are assumed as T_{max}, T_2, and T_a, respectively. The environmental cooling of Layer-II is ignored because of the rapid temperature increases. As cells closely contact each other, the heat transfer coefficient between layers (h) is similar. Then, the energy conservation equation can be expressed as

$$hA(T_{max} - T_2) = c_{LIB}m\frac{dT_2}{dt} + hA(T_2 - T_a) \tag{7}$$

Rearranging the variables and integrating Eq. (7), we have

$$\int_0^t dt = \frac{c_{LIB}m}{hA}\int_{\overline{T_{L2}}}^{T_{TR}} \frac{1}{T_{max} + T_a - 2T_2} dT_2 \tag{8}$$

where t is the propagation time for thermal runaway from Layer-I to Layer-II; and $\overline{T_{L2}}$ is the Layer-II temperature when thermal runaway of Layer-I happens. The integrating result for the propagation time is

$$t = \frac{c_{LIB}m}{2hA}\ln\left(\frac{T_{max} + T_a - 2\overline{T_{L2}}}{T_{max} + T_a - 2T_{TR}}\right) \tag{9}$$

A higher heater power will lead to a lower $\overline{T_{L2}}$, so that the propagation time is longer, resulting in a slower thermal runaway propagation rate. Continue to increase the heating power, the value of $\overline{T_{L2}}$ will reduce the ambient temperature ($\overline{T_{L2}} \rightarrow T_a$). Therefore, the propagation rate for 50% SOC cells will decrease to a constant, as shown in Fig. 10. Nevertheless, Eq. (9) is valid on premise conditions as

$$\frac{T_{max} + T_a - 2\overline{T_{L2}}}{T_{max} + T_a - 2T_{TR}} > 0 \tag{10}$$

Generally, T_{max} for low-SOC cells is relatively low, while the value of T_{TR} is high. For 30% SOC cells used in this work, the value of $T_{max} + T_a$ is lower than $2T_{TR}$ [28]. Thus, the relationship between $\overline{T_{L2}}$ and T_{max} should satisfy

$$\overline{T_{L2}} > \frac{T_{max} + T_a}{2} \tag{11}$$

It suggests that the Layer-II cells should be heated to a certain value to maintain thermal runaway propagation. In other words, the heater power should be lower to enhance the "preheating" effect. In addition, if the heater power is low enough, the thermal runaway of Layer-I cells is milder, resulting in a lower T_{max} (Fig. 9). Meanwhile, the heater will also absorb heat from Layer-I cells during the

propagation process of thermal runaway [42], due to the temperature difference between the heater and Layer-I cells (Fig. 11c). Consequently, Layer-II cells cannot gain enough heat to reach the thermal runaway threshold. Therefore, thermal runaway propagation for 30% SOC only occurs when the heater power is in a proper range in Fig. 10.

The above assumptions and simplified models are intended to explain the experimental phenomena and enhance comprehension of the heater power effect on thermal runaway propagation. Nevertheless, the present work offers a new perspective on selecting the heater power for thermal runaway propagation tests using low-SOC cells.

4.2. Selection of test heating power

The increasing global demand for LIBs pushes us to expedite safety testing and standardization processes. Thermal runaway propagation tests aim to simulate potentially worst scenarios and to develop effective countermeasures. In the literature, high heating power is typically recommended to induce the rapid thermal runaway of active high SOC cells [42]. This is because high heating power can trigger thermal runaway with less external energy input, thus increasing test repeatability and accuracy.

However, this work finds that employing extremely high heating power may not evaluate the most dangerous conditions for cells with low SOC. For cells with 50% SOC, the heating power has little effect on the thermal runaway propagation when it exceeds a certain value. Similarly, for the 30% SOC cells commonly employed in storage and transport, neither too high nor too low heating power can trigger thermal runaway propagation. According to our simplified theoretical model, heating power has a more intricate effect on the thermal runaway propagation of low-SOC cells. Generally, lower SOC cells have higher thermal runaway temperatures and lower maximum temperatures. If the heating power is too high, the second row of cells may not be sufficiently preheated, making it challenging to attain a higher thermal runaway trigger temperature. Conversely, if the heating power is too low, the lower temperature of the heater will absorb heat after the thermal runaway of Layer-I, resulting in insufficient energy to drive thermal runaway propagation.

Thus, this work proposes a new approach to select heating power, which considers both preheating and heat absorption of the heater comprehensively. Specifically, the heater power should achieve the T_{TR} when the Layer-I cells reach thermal runaway, which can roughly be estimated based on the heating time in Eq. (5). In this work, the recommended heater powers for cells with 75% SOC, 50% SOC, and 30% SOC are 300 W, 200 W, and 100 W, respectively. This approach reduces additional energy input and helps the heater to simulate a failed battery better.

It is worth noting that the energy density of the cells employed in this study is relatively lower than that of most advanced 18650-type cells. Nevertheless, the heating-power impact on thermal runaway propagation can be extrapolated to other battery cells, and we plan to investigate the specific thresholds for various cell types in future research.

4.3. Implications and challenges

Inspired by our research findings, employing heat flux as a measure of thermal impact can enhance the reliability of tests assessing the thermal runaway propagation. One significant limitation of using heating power is its lack of space dimensions. Heating power cannot be universally applied to standard thermal runaway tests conducted on cells of varying sizes, particularly for large-format cells used in energy storage systems. It has been demonstrated in several previous studies that employing the same heating power to initiate thermal runaway with different heating areas yields disparate results (Fig. 12a). Consequently, it is more reasonable to employ heat flux to quantify the ignition power [56,57].

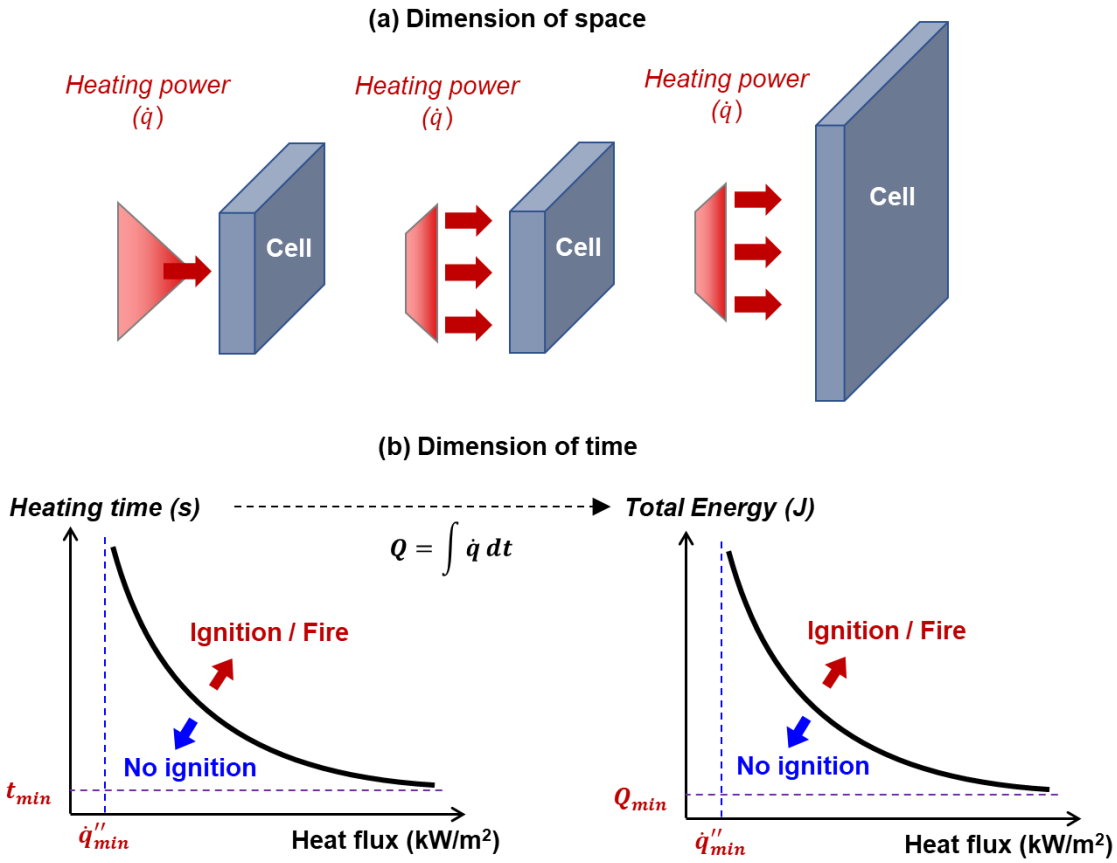

Fig. 12. The (a) space and (b) time dimensions should be considered for the thermal-runaway inducement.

Additionally, the time dimension is also crucial when inducing thermal runaway. Fig. 12b elucidates the relationship between heating time and heat flux, as well as the correlation between input energy and heat flux. To successfully ignite a fire, the minimum heat flux and heating time values should be considered. For example, using an extremely strong heat flux in a very short time will not ignite a fire due to insufficient preheating. By integrating, the curve illustrating the relationship between input energy and heat flux can be obtained. This curve also highlights two limiting conditions: minimum heat flux and minimum input energy required for ignition. Therefore, incorporating heat flux and total energy input can describe both space and time dimensions, which are essential for triggering thermal runaway and could help to promote the standard tests for thermal runaway propagation.

5. Conclusions

This work conducts a series of experiments to explore the characteristics of thermal runaway and its propagation within a rectangular LIB pile consisting of three layers. The thermal runaway of Layer-I cells is triggered by a cylindrical heater. The influences of heater power (50 W ~ 300 W) and SOC (30% ~ 75%) on thermal runaway initiation and its propagation are analyzed. Results show that the effective heating power is insensitive to the SOC level, where the heating efficiency to a single cell is around 15%. Higher heating power and higher SOC can lead to a quick trigger for thermal runaway. The low heating power can prolong the time interval between safety venting and thermal runaway, resulting in a milder thermal runaway and lower maximum temperature of failed cells.

The heater was turned off when the Layer-I cells reached thermal runaway. A specifically defined propagation rate of thermal runaway was employed to evaluate the fire hazards. As expected, the thermal runaway propagation rate increases with SOC levels. Notably, heating power has a more intricate effect on the thermal runaway propagation rate. For cells with 75% SOC, the propagation rate decreases with heating power, ascribed to the "preheating" effect. For 50% SOC cells with a relatively low thermal runaway intensity, the "preheating" effect is negligible when the heater power exceeds 150 W. Regarding 30% SOC cells, thermal runaway propagation only occurs with the heater power ranging from 75 W to 150 W. Based on the theoretical heat transfer model, two underlying factors of insufficient preheating and thermal-runaway intensity are explicitly revealed. Finally, new insights for selecting appropriate heater power are proposed, which can guide optimizing heating test procedures in the safety regulations of LIB modules.

CRediT authorship contribution statement

Yanhui Liu: Data curation, Investigation, Writing - Original Draft, Formal analysis. **Zhang Lei:** Data curation, Investigation. **Yifei Ding:** Data curation. **Xianjia Huang:** Resources, Supervision. **Xinyan Huang:** Conceptualization, Methodology, Funding acquisition, Supervision, Writing − review & editing.

Acknowledgments

This work is financially supported by the National Key Research and Development Program (Grant No. 2022YFE0207400), Early Career Scheme of Hong Kong Research Grant Council (Grant No. 25205519), and Shenzhen Science and Technology Program (Grant No. JCYJ20210324131006017).

References

[1] Feng X, Ren D, He X, Ouyang M. Mitigating Thermal Runaway of Lithium-Ion Batteries. *Joule* 2020;4:743–70.

[2] Kvasha A, Gutiérrez C, Osa U, de Meatza I, Blazquez JA, Macicior H, et al. A comparative study of thermal runaway of commercial lithium ion cells. *Energy* 2018.

[3] Xu B, Lee J, Kwon D, Kong L, Pecht M. Mitigation strategies for Li-ion battery thermal runaway: A review. *Renewable and Sustainable Energy Reviews* 2021;150:111437.

[4] Baird AR, Archibald EJ, Marr KC, Ezekoye OA. Explosion hazards from lithium-ion battery vent gas. *Journal of Power Sources* 2020;446:227257.

[5] Zhu X, Wang Z, Wang Y, Wang H, Wang C, Tong L, et al. Overcharge investigation of large format lithium-ion pouch cells with Li(Ni 0.6 Co 0.2 Mn 0.2)O 2 cathode for electric vehicles: Thermal runaway features and safety management method. *Energy* 2019;169:868–80.

[6] Finegan DP, Darcy E, Keyser M, Tjaden B, Heenan TMM, Jervis R, et al. Characterising thermal runaway within lithium-ion cells by inducing and monitoring internal short circuits. *Energy & Environmental Science* 2017;10:1377–88.

[7] Walker WQ, Cooper K, Hughes P, Doemling I, Akhnoukh M, Taylor S, et al. The effect of cell geometry and trigger method on the risks associated with thermal runaway of lithium-ion batteries. *Journal of Power Sources* 2022;524:230645.

[8] Duh YS, Liu X, Jiang X, Kao CS, Gong L, Shi R. Thermal kinetics on exothermic reactions of a commercial LiCoO2 18650 lithium-ion battery and its components used in electric vehicles: A review. *Journal of Energy Storage* 2020;30:101422.

[9] Jia Y, Darst J, Surelia A, Delafuente D, Finegan DP, Xu J. Deformation and fracture behaviors of cylindrical battery shell during thermal runaway. *Journal of Power Sources* 2022;539:231607.

[10] Liu F, Wang J, Yang N, Wang F, Chen Y, Lu D, et al. Experimental study on the alleviation of thermal runaway propagation from an overcharged lithium-ion battery module using different thermal insulation layers. *Energy* 2022;257:124768.

[11] Wang Q, Mao B, Stoliarov SI, Sun J. A review of lithium ion battery failure mechanisms and fire prevention strategies. *Progress in Energy and Combustion Science* 2019;73:95–131.

[12] Abada S, Petit M, Lecocq A, Marlair G, Sauvant-Moynot V, Huet F. Combined experimental and modeling approaches of the thermal runaway of fresh and aged lithium-ion batteries. *Journal of Power Sources* 2018;399:264–73.

[13] Kong D, Wang G, Ping P, Wen J. A coupled conjugate heat transfer and CFD model for the thermal runaway evolution and jet fire of 18650 lithium-ion battery under thermal abuse. *ETransportation* 2022;12:100157.

[14] Mishra D, Jain A. Multi-mode heat transfer simulations of the onset and propagation of thermal runaway in a pack of cylindrical li-ion cells. *Journal of The Electrochemical Society* 2021;168:20504.

[15] Tran M-K, Bhatti A, Vrolyk R, Wong D, Panchal S, Fowler M, et al. A Review of Range Extenders in Battery Electric Vehicles: Current Progress and Future Perspectives. *World Electric Vehicle Journal* 2021;12.

[16] Sun P, Bisschop R, Niu H, Huang X. A Review of Battery Fires in Electric Vehicles. *Fire Technology* 2020;56:1361–410.

[17] Zhang W, Huang L, Zhang Z, Li X, Ma R, Ren Y, et al. Non-uniform phase change material strategy for directional mitigation of battery thermal runaway propagation. *Renewable Energy* 2022;200:1338–51.

[18] Zhou Z, Zhou X, Ju X, Li M, Cao B, Yang L. Experimental study of thermal runaway propagation along horizontal and vertical directions for LiFePO4 electrical energy storage modules. *Renewable Energy* 2023;207:13–26.

[19] Li K, Wang H, Xu C, Wu W, Zhang W, Hou J, et al. Multi-objective optimization of side plates in a large format battery module to mitigate thermal runaway propagation. *International Journal of Heat and Mass Transfer* 2022;186:122395.

[20] Liu L, Lin C, Fan B, Wang F, Lao L, Yang P. A new method to determine the heating power of ternary cylindrical lithium ion batteries with highly repeatable thermal runaway test characteristics. *Journal of Power Sources* 2020;472:228503.

[21] Lai X, Wang S, Wang H, Zheng Y, Feng X. Investigation of thermal runaway propagation characteristics of lithium-ion battery modules under different trigger modes. *International Journal of Heat and Mass Transfer* 2021;171:121080.

[22] Said AO, Lee C, Stoliarov SI, Marshall AW. Comprehensive analysis of dynamics and hazards associated with cascading failure in 18650 lithium ion cell arrays. *Applied Energy* 2019;248:415–28.

[23] Lopez CF, Jeevarajan JA, Mukherjee PP. Experimental analysis of thermal runaway and propagation in lithium-ion battery modules. *Journal of the Electrochemical Society* 2015;162:A1905–15.

[24] Fang J, Cai J, He X. Experimental study on the vertical thermal runaway propagation in cylindrical Lithium-ion batteries: Effects of spacing and state of charge. *Applied Thermal Engineering* 2021;197:117399.

[25] Weng J, Yang X, Ouyang D, Chen M, Zhang G, Wang J. Comparative study on the transversal/lengthwise thermal failure propagation and heating position effect of lithium-ion batteries. *Applied Energy* 2019;255:113761.

[26] Zhong G, Li H, Wang C, Xu K, Wang Q. Experimental analysis of thermal runaway propagation risk within 18650 lithium-ion battery modules. *Journal of the Electrochemical Society* 2018.

[27] Weng J, Ouyang D, Liu Y, Chen M, Li Y, Huang X, et al. Alleviation on battery thermal runaway propagation: Effects of oxygen level and dilution gas. *Journal of Power Sources* 2021;509:230340.

[28] Liu Y, Niu H, Liu J, Huang X. Layer-to-layer thermal runaway propagation of open-circuit cylindrical li-ion batteries: Effect of ambient pressure. *Journal of Energy Storage* 2022;55:105709.

[29] Wang Z, Jiang X, Ke W, Wang W, Zhang S, Zhou B. Effect of lithium-ion battery diameter on thermal runaway propagation rate under one-dimensional linear arrangement. *Thermal Science and Engineering Progress* 2022;31:101301.

[30] Yan W, Wang Z, Ouyang D, Chen S. Analysis and prediction of thermal runaway propagation

interval in confined space based on response surface methodology and artificial neural network. *Journal of Energy Storage* 2022;55:105822.

[31] Huang Y, Lu J, Lu Y, Liu B. Investigation into the effects of emergency spray on thermal runaway propagation within lithium-ion batteries. *Journal of Energy Storage* 2023;66:107505.

[32] Liu Y, Niu H, Xu C, Huang X. Thermal runaway propagation in linear battery module under low atmospheric pressure. *Applied Thermal Engineering* 2022;216:119086.

[33] Wang H, Shi W, Hu F, Wang Y, Hu X, Li H. Over-heating triggered thermal runaway behavior for lithium-ion battery with high nickel content in positive electrode. *Energy* 2021;224:120072.

[34] Li K, Xu C, Wang H, Jin C, Rui X, Chen S, et al. Investigation for the effect of side plates on thermal runaway propagation characteristics in battery modules. *Applied Thermal Engineering* 2022;201:117774.

[35] Li Z, Zhang P, Shang R. Effects of heating position on the thermal runaway propagation of a lithium-ion battery module in a battery enclosure. *Applied Thermal Engineering* 2023;222:119830.

[36] Niu H, Chen C, Liu Y, Li L, Li Z, Ji D, et al. Mitigating thermal runaway propagation of NCM 811 prismatic batteries via hollow glass microspheres plates. *Process Safety and Environmental Protection* 2022;162:672–83.

[37] Shen K, Mao Y, Zheng Y, Yang W, Wu B. One-Dimensional Modeling and Experimental Analysis of Nail Penetration Thermal Runaway for Large Capacity Li-Ion Power Battery. *Journal of The Electrochemical Society* 2022;169:040502.

[38] Jin C, Sun Y, Wang H, Lai X, Wang S, Chen S, et al. Model and experiments to investigate thermal runaway characterization of lithium-ion batteries induced by external heating method. *Journal of Power Sources* 2021;504:230065.

[39] World Trade Organization Technical Barriers to Trade (TBT) Committee. E1321-18 Standard Test Method for Determining Material Ignition and Flame Spread Properties. 2018.

[40] Huang Z, Shen T, Jin K, Sun J, Wang Q. Heating power effect on the thermal runaway characteristics of large-format lithium ion battery with Li(Ni1/3Co1/3Mn1/3)O2 as cathode. *Energy* 2022;239:121885.

[41] Wang H, Xu H, Zhao Z, Wang Q, Jin C, Li Y, et al. An experimental analysis on thermal runaway and its propagation in Cell-to-Pack lithium-ion batteries. *Applied Thermal Engineering* 2022;211:118418.

[42] Jin C, Sun Y, Wang H, Zheng Y, Wang S, Rui X, et al. Heating power and heating energy effect on the thermal runaway propagation characteristics of lithium-ion battery module: Experiments and modeling. *Applied Energy* 2022;312:118760.

[43] Wang H, Wang Q, Zhao Z, Jin C, Xu C, Huang W, et al. Thermal runaway propagation behavior of the Cell-to-Pack battery system. *Journal of Energy Chemistry* 2023;84:162–72.

[44] Choudhari V, Dhoble AS, Panchal S, Fowler D, Fraser D. Experimental and Numerical Investigation on Thermal Characteristics of 2× 3 Designed Battery Module. *Available at SSRN* n.d.

[45] Liu T, Hu J, Tao C, Zhu X, Wang X. Effect of parallel connection on 18650-type lithium ion battery thermal runaway propagation and active cooling prevention with water mist. *Applied Thermal Engineering* 2021;184:116291.

[46] Liu Y, Aldan G, Huang X, Hao M. Single-phase static immersion cooling for cylindrical lithium-ion battery module. *Applied Thermal Engineering* 2023;233:121184).

[47] Liu Y, Niu H, Li Z, Liu J, Xu C, Huang X. Thermal runaway characteristics and failure criticality of massive ternary Li-ion battery piles in low-pressure storage and transport. *Process Safety and Environmental Protection* 2021;155:486–97.

[48] Zhao J, Xue F, Fu Y, Cheng Y, Yang H, Lu S. A comparative study on the thermal runaway inhibition of 18650 lithium-ion batteries by different fire extinguishing agents. *IScience* 2021;24:102854.

[49] Huang P, Yao C, Mao B, Wang Q, Sun J, Bai Z. The critical characteristics and transition process of lithium-ion battery thermal runaway. *Energy* 2020;213:119082.

[50] Zhou Z, Zhou X, Cao B, Yang L, Liew KM. Investigating the relationship between heating temperature and thermal runaway of prismatic lithium-ion battery with LiFePO4 as cathode. *Energy* 2022;256:124714.

[51] Quintiere JG. On methods to measure the energetics of a lithium ion battery in thermal runaway. *Fire Safety Journal* 2020;111:102911.

[52] Zhang Q, Liu T, Wang Q. Experimental study on the influence of different heating methods on thermal runaway of lithium-ion battery. *Journal of Energy Storage* 2021;42:103063.

[53] Li K, Li Y, Rui X, Cao Y, Fan L, Feng X. Experimental study on the effect of state of charge on failure propagation characteristics within battery modules. *Chinese Journal of Electrical Engineering* 2023:1–12.

[54] Fu Y, Lu S, Shi L, Cheng X, Zhang H. Ignition and combustion characteristics of lithium ion batteries under low atmospheric pressure. *Energy* 2018;161:38–45.

[55] Quintiere JG. Fundamentals of Fire Phenomena. London: John Wiley & Sons, Ltd; 2006.

[56] Zhou Z, Ju X, Zhou X, Yang L, Cao B. A comprehensive study on the impact of heating position on thermal runaway of prismatic lithium-ion batteries. *Journal of Power Sources* 2022;520:230919.

[57] Huang Z, Yu Y, Duan Q, Qin P, Sun J, Wang Q. Heating position effect on internal thermal runaway propagation in large-format lithium iron phosphate battery. *Applied Energy* 2022;325:119778.

Appendix

Table A1 shows the selection of heater power based on GB 38031-2020. Fig. A1 compares the experimental phenomena of battery modules at (a) 75% SOC and (b) 30% SOC with a 200-W heater. Fig. A2 demonstrates the temperature evolution curves of the battery module at (a) 75% SOC and (b) 30% SOC, where the heater power is 200 W.

Table A1. The heater power selection recommended by GB 38031-2020.

Energy of the cell (Wh)	$E < 100$	$100 \leq E < 400$	$400 \leq E < 800$	$E \geq 800$
Maximum heater power (W)	30~300	300~1000	300~2000	>600

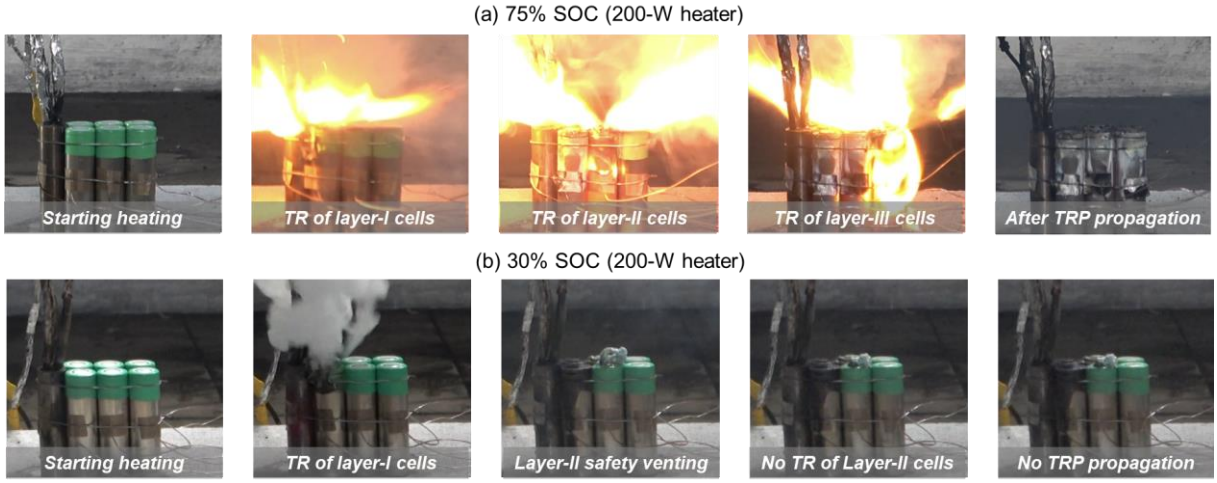

Fig. A1. Experimental observations of battery modules at (a) 75% SOC and (b) 30% SOC with a 200-W heater.

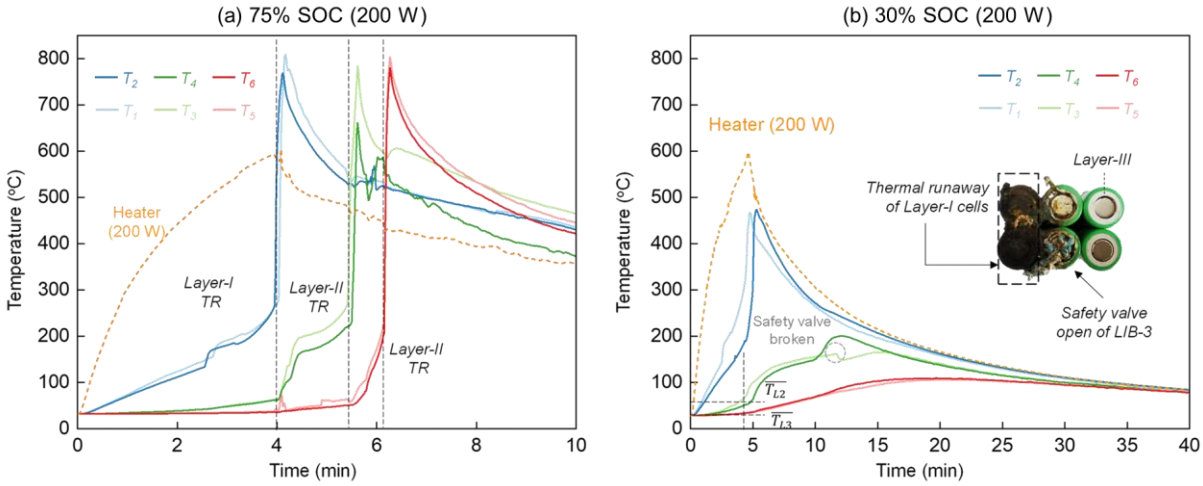

Fig. A2. Temperature curves of the battery modules at (a) 75% SOC and (b) 30% SOC with a 200-W heater.